



High sensitive polyaniline nanosheets (PANINS) @rGO as non-enzymatic glucose sensor

Saraswathi Kailasa¹ · R. Kiran Kumar Reddy¹ · M. Sai Bhargava Reddy¹ · B. Geeta Rani¹ · Hussien Maseed² · R. Sathyavathi³ · K. Venkateswara Rao¹

Received: 16 October 2019 / Accepted: 27 December 2019 / Published online: 9 January 2020
© Springer Science+Business Media, LLC, part of Springer Nature 2020

Abstract

This study aims the amperometric enzyme-free glucose sensing of interlayered Polyaniline nanosheets @reduced grapheme oxide (PANINS@rGO). Conductive PANINS were synthesized using in situ chemical oxidative polymerization method. The PANINS@rGO nanocomposite was prepared by the solution mixing method and as-synthesized material was fully examined using various spectroscopy and microscopy techniques. PANINS@rGO composite coated on screen-printed carbon electrode (SPCE) was studied for electrochemical behaviour for the detection of non-enzymatic glucose. The fabricated sensor matrix was tested towards detection of glucose efficacy using cyclic voltammetry (CV) and Chronoamperometry (CA) techniques in the presence of 0.1 M NaOH electrolyte in a range of 1–10 mM at an optimum working potential of 60 mV s⁻¹. PANINS@rGO/SPCE absorbed with high sensitivity (3448.27 $\mu\text{A mM}^{-1} \text{cm}^{-2}$) and excellent low detection limit (LOD) 30 nM, (S/N = 3). Furthermore, the obtained results of the proposed PANINS@rGO/SPCE fabricated a finite sensor for non-enzymatic glucose sensor. Thus this report proves the practical opportunities for the development of environmentally benign, cost effective and chemically stable electrode materials for sensors, which may be beneficial for the expansion of economically viable enzyme free electrochemical glucose sensor devices.

1 Introduction

Diabetes mellitus is one of the major issues in clinical diagnostics for accurate determination of glucose concentration [1–6]. Despite the lack of a sophisticated cure for diabetes mellitus, the desire for continuous monitoring of blood glucose levels has prompted demand for low cost, reliable and accurate glucose detection. Hence, a lot of industries such as clinical, biological, chemical diagnosis and food industries are concentrating on monitoring the glucose levels. Later

many methodologies have been developed by researchers across the globe to enhance the glucose monitoring such as electronic, optical, fluorescent, transdermal and electrochemical methods, where electrochemical sensors gained huge attention due to low cost and easy synthesis [7–12]. Electrochemical glucose sensors are mainly enzyme and non-enzyme based. Electrochemical enzyme-based sensors show high selectivity and sensitivity; however, poor stability, slow electrode kinetics, reproducibility, temperature, pH and high-cost complications appear with enzymatic glucose sensors [13–15]. Therefore, the simple reliable, low cost and better stability sensor matrix required for accurate glucose detection with direct electro-oxidation also called non-enzymatic glucose sensing [16]. Recent studies have shown that non-enzymatic glucose detection technique is one of the most promising approaches than traditional Colorimetry (usage of blood test) and high-performance liquid chromatography (HPLC), due to its very low levels detection (10^{-9} to 10^{-13} g), high selectivity, low cost and ease of operation.

Graphene, a fascinating two dimensional (2D) carbon material, has emerged as future material for the electrochemical applications such as batteries, supercapacitor and

Electronic supplementary material The online version of this article (<https://doi.org/10.1007/s10854-019-02837-1>) contains supplementary material, which is available to authorized users.

✉ K. Venkateswara Rao
kalagadda2003@gmail.com

¹ Center for Nanoscience and Technology, Institute of Science and Technology, Jawaharlal Nehru Technological University, Telangana State, Hyderabad 500085, India

² School of Engineering Sciences and Technology, University of Hyderabad, Gachibowli, Hyderabad 500046, India

³ Department of Physics, Koneru Lakshmaiah Education Foundation (KLEF), Hyderabad 500075, India

non-enzymatic glucose sensing due to its exceptional electrical, mechanical, thermal properties and high surface area. Besides, rGO helps to connect more active sites that tightly joining the polymer nanoparticles, which possibly prevents the agglomeration of the active nanomaterials during the redox and catalytic process [17].

In earlier, many enzyme-free glucose sensors have been made based on the metal oxide NPs [18, 19], metal NPs [20, 21], polymer nanostructures [22], carbon-based materials and composites [23]. Among all these materials, conducting polymers received huge attention because of its ease of synthesis, tuneable electronic conductivity, excellent mechanical strength, environmental stability, reversible doping/de-doping chemistry, versatile electrochemical switching behaviour and suitability for making composites with different types of binders. Moreover, metals conduct electricity via electrons in the conduction band that travels across atoms in the lattice, while inorganic materials conductivity occurs by the mobility of the delocalized π -electrons along the polymer chain [24, 25]. Among the various conductive polymers (CPs), PANI has gained much more attention because it is a phenyl-based polymer having chemically flexible $-\text{NH}$ group in polymer chain flanked either side by phenylene ring; this is responsible for protonation, deprotonation and various other physicochemical properties. PANI is an oxidative polymeric product of aniline under acidic conditions [26–32]. However, lack of solubility is one of the major drawbacks of PANI because of its stiffness of backbone and H-bonding interactions between chains of adjacent [25]. Over a decade, many researchers demonstrated that PANI showed good conductivity in organic solvents such as NMP, DMSO, DMF and Camphor sulphuric acid [33–35] which showed improved processibility, spectroscopic, electrical and optical properties.

To the best of our knowledge, till date no reports available based on PANINS@rGO composite coated on SPCE prepared for the detection of non-enzymatic glucose for the first time. Firstly, PANINS were synthesized from in situ polymerization and rGO was reduced through the hydrothermal method. The PANINS@rGO composite obtained through solution mixing procedure. This process involves the dispersion of NPs in a polymer solution followed by drying of the solvent. This process requires extensive mixing/sonication to disperse NPs homogeneously in the polymer matrix for 8 h to avoid agglomeration that can sometimes occur by resulting non-homogeneous distribution of NPs. The fabricated PANINS@rGO sensor matrix shows better selectivity, sensitivity and low detection limit towards an enzyme-free glucose sensing.

2 Experimental

2.1 Materials and apparatus

Graphite Flakes (GFs), Sulphuric acid (H_2SO_4), Sodium nitrate (NaNO_3), Hydrogen Peroxide (H_2O_2), Potassium permanganate (KMnO_4), Aniline obtained from Sigma-Aldrich. Ammonium persulfate [$(\text{NH}_4)_2\text{S}_2\text{O}_8$], Hydrochloric Acid (HCl), Sodium dodecyl sulphate (SDS), Ethanol, *N*-methyl-2-pyrrolidone (NMP), Sodium hydroxide (NaOH), Dimethyl formamide (DMF), Ascorbic acid (AA), Dimethyl sulphoxide (DMSO) Glucose, Fructose, Maltose, Lactose, Galactose were of analytical grade and were used without any further processing. The screen-printed Carbon electrodes (SPCE) purchased from DropSens (Spain).

2.2 Electrochemical experiments

All electrochemical experiments including cyclic voltammetry (CV) and chronoamperometry were performed on METROHM Auto lab (JNT University Hyderabad) PGSTAT-302N (Potentiostat/Galvanostat) with electrochemical USB interface and run by NOVA software (Eco Chemie, Netherlands) also have screen printed three electrode strip connector and a computer for storage and processing purpose. SPCE is composed of three interdigitated electrodes with a 4 mm diameter, graphite working electrode (WE), graphite counter electrode (CE) and silver/silver chloride (Ag/AgCl) as a reference electrode (RE). All the experiments were done at room temperature.

2.3 Physical characterization

The GO has been synthesized using modified hummers method further reduced with the help of the hydrothermal technique. The polyaniline nanosheets were prepared by in situ polymerization. The as-obtained samples were characterized with help of XRD to find out the crystallinity with Bruker D8 X-ray diffractometer ($\text{Cu K}\alpha$; $\lambda = 1.5418 \text{ \AA}$). A field emission scanning electron microscope (FESEM) and transmission electron microscope (TEM) were employed for the surface morphology analysis of obtained nanostructures. The functional groups were confirmed using (Perkin-Elmer-FTIR Spectrum-100) Fourier transform infrared spectroscopy with wavelength range $500\text{--}4500 \text{ cm}^{-1}$. The solubility and absorbance were characterized using UV-Vis spectrophotometer 2202 (Systronics Double Beam).

2.4 Synthesis of interlayered polyaniline nanosheets (PANINS)/rGO

2.4.1 Synthesis of PANINS

For the past few decades, the tuned synthesis of Polyaniline nanostructures with unique morphologies has acknowledged huge attention [36–42]. The conductive PANINS were prepared using in situ chemical oxidative polymerization method. Firstly, Aniline hydrochloride solution is prepared by adding aniline monomer at different ratios 1:10:3 to 100 mL DI water and stirred for 15 min in the presence of ice bath, followed by the addition of SDS to aniline, and stirring was continued for another 15 min; the temperature was maintained around 5 °C. Separately, (1:2) molar ratio of aniline and $(\text{NH}_4)_2\text{S}_2\text{O}_8$, an oxidizing agent solution was prepared and added slowly, by drop wise to aniline—hydrochloride resulted solution changes its colour from yellow to blue then green colour, specifies the formation of PANI. The solution was allowed to stand for 48 h at room temperature. The green colloidal solution was precipitated by addition of acetone and filtered to obtain residue. It was washed for several times with acetone, ethanol and DI water until the

filtrate was colourless. The precipitate was dried in an oven at 60 °C for 14 h and then ground into a mortar–pestle into a fine green powder to obtain conductive PANINS (Emeraldine salt) [43] as shown in Fig. 1b.

2.4.2 Synthesis of reduced graphene oxide

Figure 1b illustrates the synthesis of GO using a modified Hummers method with slight modifications, and it was reduced using Hydrothermal method by few steps. In the first step, the as-obtained 2 g of GFs and 1 g of NaNO_3 were uniformly mixed in 90 mL of concentrated H_2SO_4 in 500 mL beaker for 30 min. In the second step, 7 g of KMnO_4 was slowly added to the above slurry in presence of an ice bath to maintain temperature less than 15 °C. After that, DI water was slowly added to reaction mixture and its internal temperature was raised up to 98 °C. Then the solution was stirred for 60 min at 800 rpm using magnetic stirrer at room temperature until a thick paste material is formed. In the third step, 3 mL of H_2O_2 was slowly added to that above suspension to stop the reaction and then the colour of reaction mixture changed from brown to yellow. The as-prepared GO paste washed with DI water for several times until pH

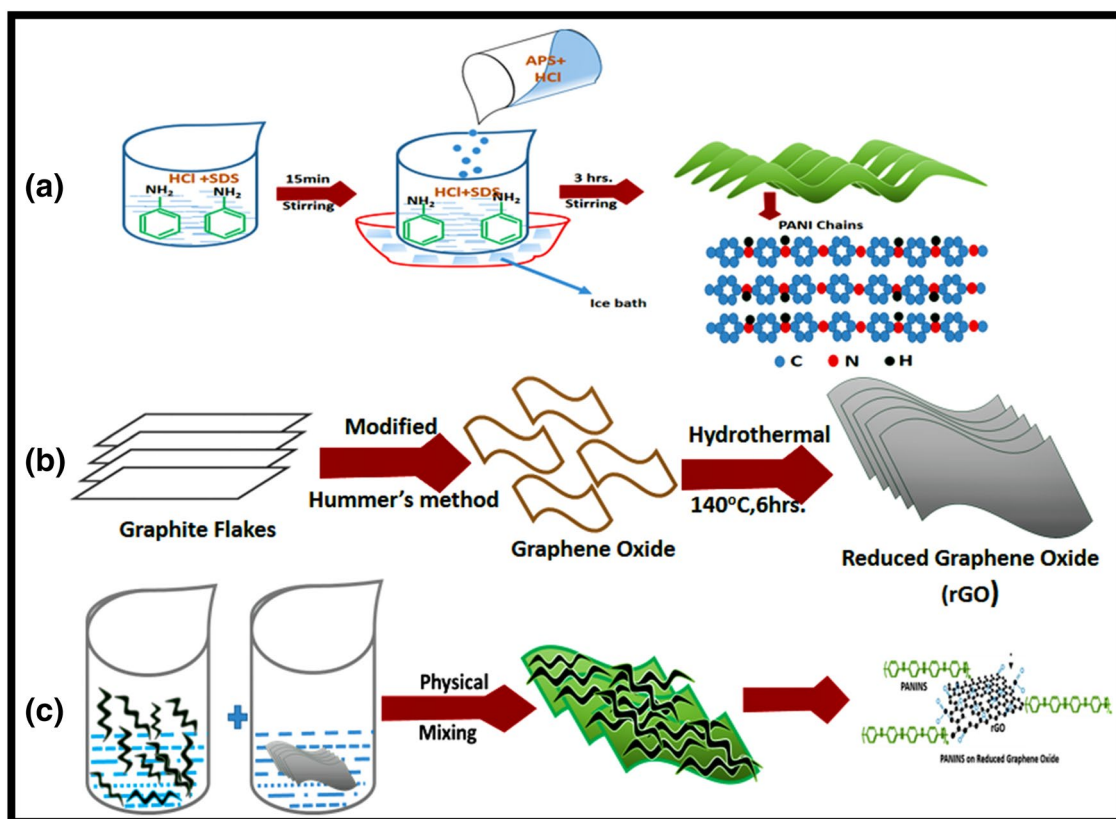


Fig. 1 Schematics of **a** synthesis of Polyaniline nanosheets (PANINS) **b** Preparation of GO by modified Hummers method and reduction by hydrothermal **c** formation of PANINS@rGO by solution mixing method

becomes neutral. It was centrifuged at 5000 rpm for several times with DI water and 10% HCl to remove unreacted products. The collected paste was dried in a vacuum oven overnight at 90 °C to get powdered GO [44]. The obtained GO was dispersed in DI water and it was ultrasonicated for 30 min to get a uniform brown colour suspension. Then this suspension is transferred to Teflon autoclave (100 mL) and maintained the temperature at 140 °C for 6 h. After that, it was allowed to cool down to room temperature. The final product was washed with DI water and dried at 90 °C for 10 h.[45].

2.4.3 Synthesis of PANINS@rGO

0.0198 g of PANINS was taken in a 50-mL beaker and two portions of 1% rGO [46] in another 50-mL beaker in DI water and were magnetically stirred individually for 15 min and then solutions were mixed. This method requires extensive mixing to achieve a homogeneous dispersion of rGO in a polymer matrix for approximately 8 to 10 h in order to avoid possible agglomeration that can occur sometimes which leads to non-homogeneous dispersion of NPs in the polymer matrix as displayed in Fig. 1c. The final as-obtained product was dried at a temperature of 60 °C for 12 h to obtain PANINS@rGO composite [47].

2.5 Modified PANINS@rGO electrode fabrication and electrochemical studies

The as-prepared PANINS@rGO composite was fabricated for electrochemical determination of glucose using SPCE. Firstly, 1 mg of PANINS@rGO powder and 1% of PVDF binder were dispersed in 1 mL of NMP, and sonicated for 20 min to achieve homogeneous distribution. From this aliquot 5 μ L is dropped cast on SPCE and was allowed to dry for 12 h at room temperature. The electrochemical behaviour of PANINS@rGO-SPCE was used for non-enzymatic glucose determination using voltammetry and amperometry techniques in 0.1 M NaOH solution. The electrochemical behaviour oxidation and reduction was observed by increasing the concentration in the range from 1 to 10 mM.

3 Results and discussion

The as-synthesized nanomaterials were identified with various characterization techniques. XRD is one of the extensively using non-destructive techniques to analyse the crystallite size, orientation and average spacing of atomic layers. X-ray diffraction (XRD) patterns of the as-prepared GO, rGO, PANINS and PANINS/rGO materials are shown in Fig. 2. This GO showed reflection peak of (001) at 2 θ value of 10.5° with an interplanar (d) spacing of 0.94 nm

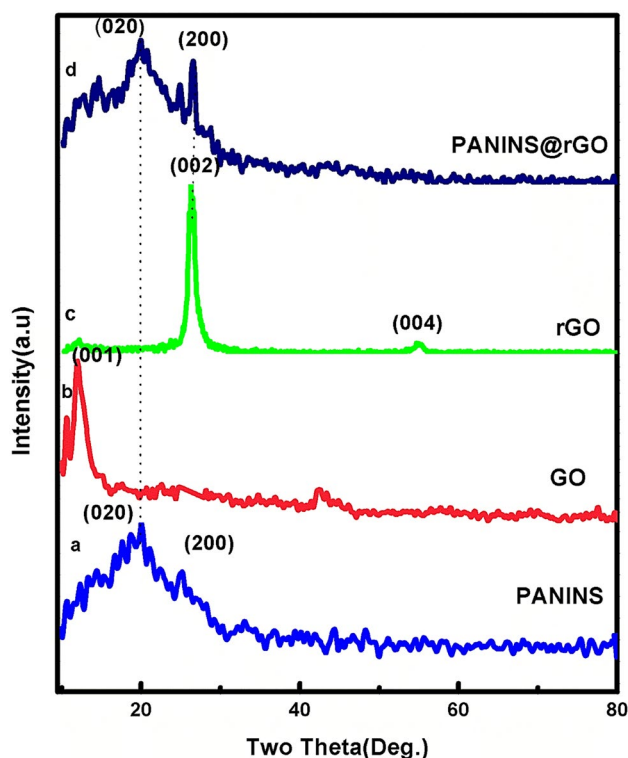


Fig. 2 XRD patterns of PANINS, GO, rGO and PANINS@rGO

which clearly indicates an oxidized form of graphite with a decoration of functional groups and it was further confirmed from FTIR spectroscopy. A broad peak was observed at 26.4° in case of rGO which confirms GO was reduced using the hydrothermal method. The 2 θ reflection peaks of PANINS at 19.84° and broad peak at 26.56° clearly indicates the formation of PANINS@rGO composite. The exhibited peaks of PANINS@rGO are observed at 19.84°, 23.86°, 26.01°, 28.01°, 32.26°, 33.03° and 38.5° reflection peaks indexed as (110), (200), (003), (210), (120), (121) (JCPDS card No. 53-1718 and 53-1890) of PANI [48]. The crystal size and d-spacing of individual materials and a clear shift in PANINS@rGO composite are shown in Table 1.

$$D = \frac{k\lambda}{\beta \cos \theta} \quad (1)$$

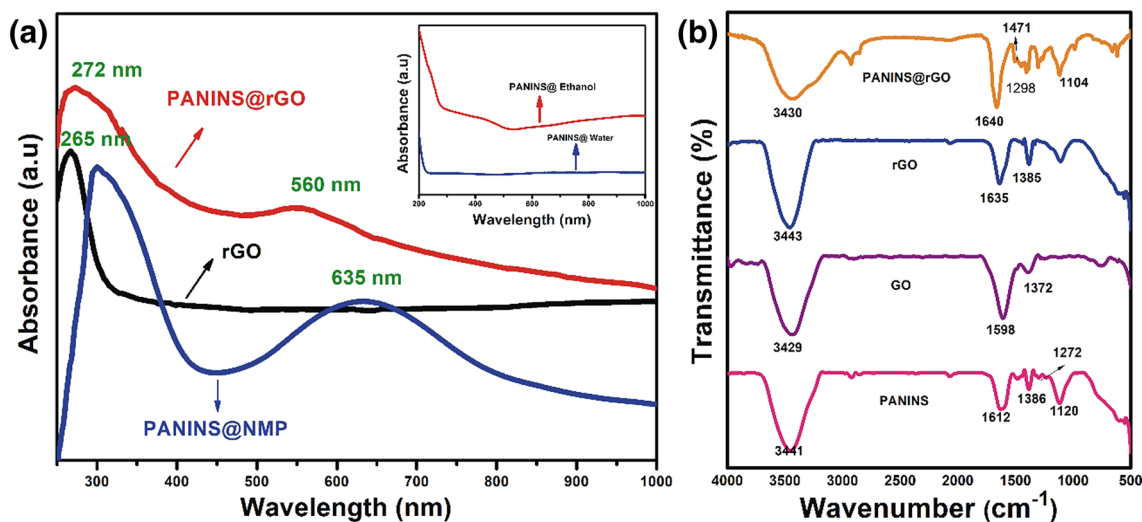
$$d = \frac{n\lambda}{2 \sin \theta} \quad (2)$$

where ‘D’ is the average crystallite size, ‘d’ is interplanar spacing, ‘ θ ’ is Bragg’s angle, ‘ λ ’ is the wavelength of X-ray and ‘ β ’ is the full width half maximum (FWHM).

The solubility of PANINS was found by dissolving in NMP, ethanol and DI water. Fig. 3a shows the absorbance of PANINS in NMP. The absorbance value is more in NMP than DI water which is in correspondence to high to low

Table 1 Crystal parameters of PANINS, rGO and rGO@PANINS

Sample name	2 θ	Crystal size $D = \frac{k\lambda}{\beta \cos \theta}$ (average) nm	d-spacing $d = \frac{n\lambda}{2 \sin \theta}$	Reference (JCPDF)	hkl
PANINS	19.26		0.4602	0.464	(110)
	26.01		0.3421	0.3406	(003)
	33.03	21	0.2708	0.2691	(120)
	38.5		0.2335	0.2331	(310)
RGO	26.4		0.3372	0.3375	(002)
	54.5	13	0.1681	0.1681	(004)
PANINS@rGO	19.84		0.4445	0.464	(110)
	26.56	15	0.3352	0.3375	(002)

**Fig. 3** **a** UV–Visible spectroscopy of PANINS, rGO and PANINS@rGO (inset: PANINS absorbance in DI water and ethanol). **b** FTIR spectroscopy of PANINS, GO, rGO, PANINS@rGO

solubility (Fig. 3a inset showing the solubility in DI water and ethanol). PANINS/NMP exhibited π – π^* transition of a benzenoid ring at 290 nm. Similarly, π – π^* transition of quinoid rings of PANINS/ NMP showed a peak at 635 nm which leads to blue shifts. Figure 3a displays absorbance of pure rGO in organic solvents exhibits at 270 nm which is responsible for π – π^* transition of aromatic $c=c$ bonds. After ultrasonication of PANINS and rGO about 8 h at 800 rpm, π – π^* transition of quinoid ring peak of PANINS in PANINS@rGO is shifted from 635 to 560 nm and rGO peak appeared at 272 nm. This is because of π – π stacking between the rGO and PANINS quinoid rings. This clearly confirms that the PANINS was stacked on the surface of rGO sheets and these results were also inter-related to XRD and FTIR absorption spectra are shown below [49, 50]. The reaction mechanism of PANINS/rGO in NMP is shown in Fig. 4.[51].

Figure 3b shows FTIR spectra of PANINS, GO, rGO, and PANINS@rGO in range of 4500–500 cm^{-1} . For the confirmation of quality of PANINS, the intense peak at 3441 cm^{-1} was attributed to N–H stretching and predominant peak

observed at 1297, 1486 and 1580 cm^{-1} are corresponding to –C–N stretching vibration, –C=C stretching vibrations in benzenoid ring and –C=C stretching of the quinoid rings, respectively, and also peak appeared at 796 cm^{-1} is attributed to C–Cl stretch (shows the Emeraldine salt). The peak of rGO at 1635 cm^{-1} is corresponding to SP^2 hybridization of carbons. PANINS@rGO contains characteristic peaks of both PANINS and rGO. The redshift occurs because of the transformation of quinoid rings into benzenoid rings and also proves π – π stacking between PANINS and rGO in PANINS@rGO. This indicated that PANINS were interlayer in between rGO successfully.

The morphological analysis of PANINS, rGO, PANINS@rGO was examined using a FESEM and TEM. Figure 5a shows the structure layer-like sheets of rGO with a diameter of 200–700 nm. This confirms that the reduction of GO through hydrothermal route was helpful and it also (corner) looks like one single fine layer was stacked with another single layer. Figure 5b displays the formation of Polyaniline nanosheets (PANINS) with sodium dodecyl sulphate which

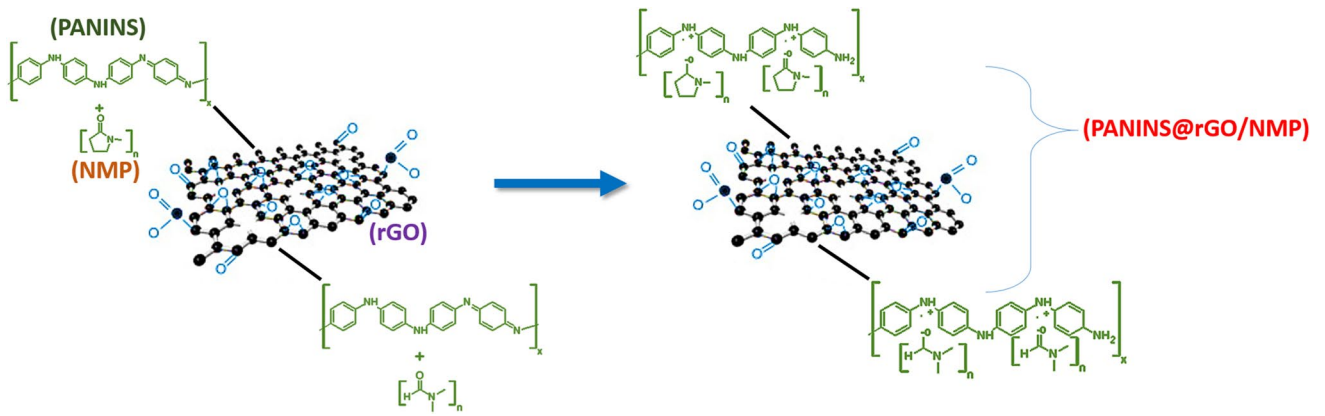


Fig. 4 Reaction of NMP with PANINS@rGO

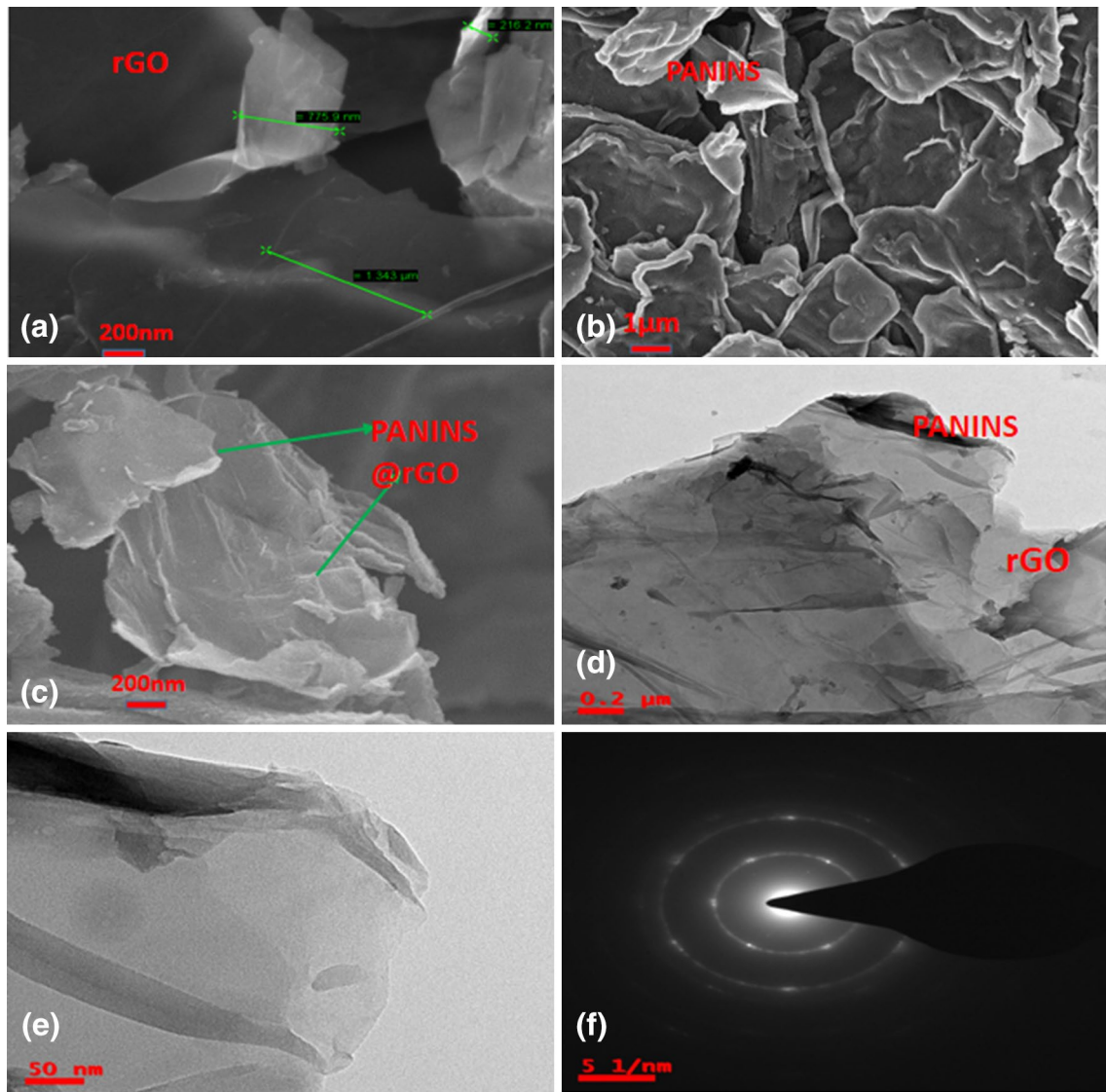


Fig. 5 a–c FESEM images of rGO, PANINS and PANINS@rGO d–f TEM images of PANINS@rGO and SEAD pattern

played as structure directing agent through in situ polymerisation and Fig. 5c–e proves the formation of interlayered PANINS @rGO composite. Polyaniline contains many sp^2 carbon atoms which encourage delocalized transport of charge carriers and may act as conducting conduits that bounds with rGO and plays as sensitizing agents to enhance the performance of the sensor. It was further confirmed from TEM. From both FESEM and TEM analysis, it was noticed that PANINS stacked on rGO sheets. The stacked PANINS size on rGO sheets is smaller and this could be useful to enhance the electrochemical utilization of PANINS for direct electron mobility during the glucose oxidation. Moreover, an rGO sheet is used due to the large surface area and also helps to increase the conductivity of the composite. Figure 5f shows the selected area electron diffraction (SAED) which reveals the increased crystalline nature of composite. These results were interconnected with XRD and FTIR results.

3.1 Electrochemical characterization

The electrochemical analysis of synthesized materials of PANINS@rGO was performed at room temperature in the presence of 0.1 M NaOH which are shown in Fig. 6a. No characteristic response is observed in the presence and absence of glucose for unmodified SPCE, whereas PANINS@rGO-modified SPCE showed characteristic peaks towards glucose oxidation at 20 mV s^{-1} scan rate with a potential window of -0.2 to 0.8 V . Figure 6a shows CVs of PANINS@rGO/SPCE with onset potential of 0.056 V , and maximum peak potential was noted at 0.50 V . In the presence of glucose, oxidation is happening towards with inset potential of 0.047 V and maximum peak potential was observed at 0.48 V . The decrease in peak potential of glucose oxidation of PANINS@rGO/SPCE surface proves the improved electrocatalytic activity. The significant improvement in the current is due to solubility of PANI

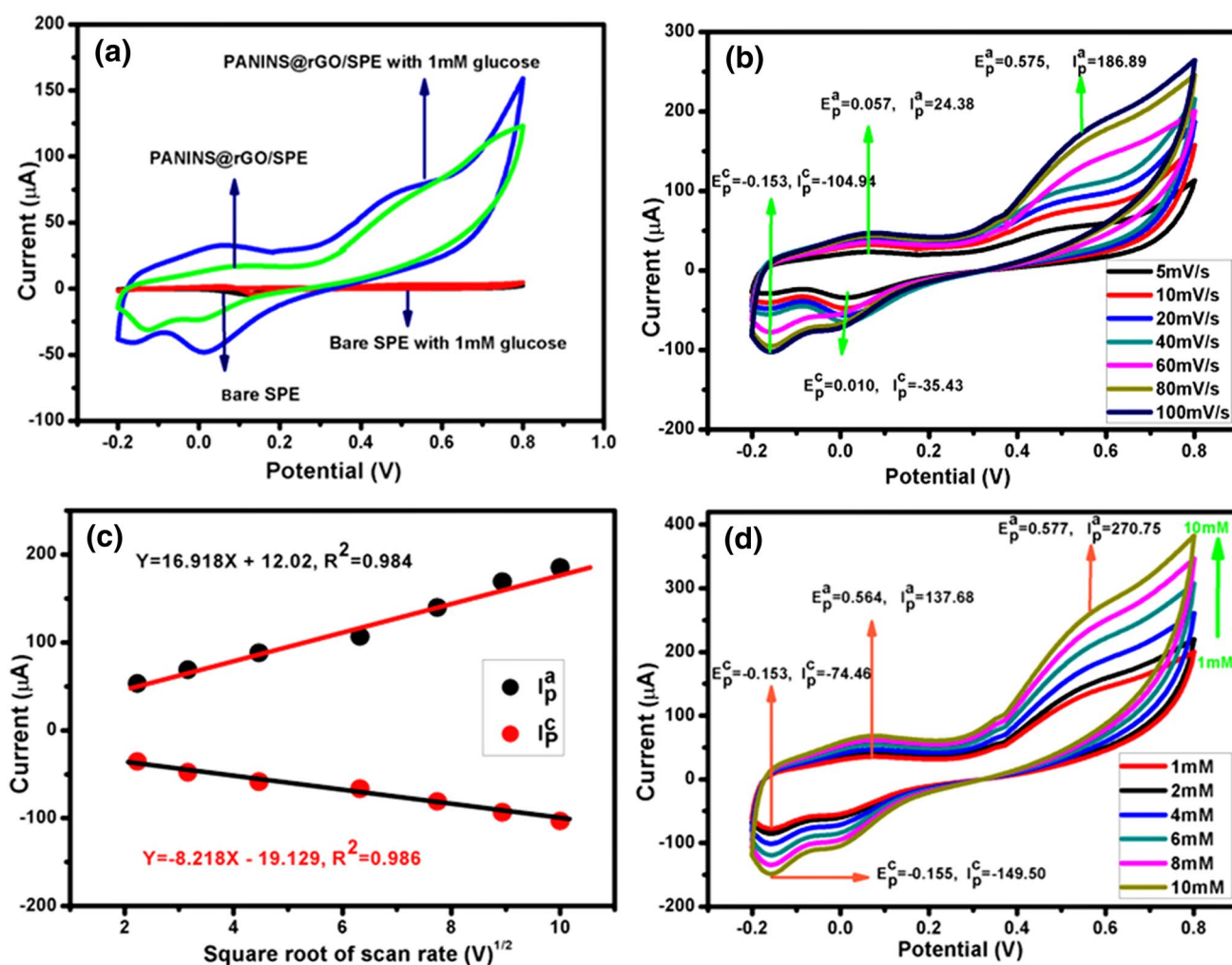


Fig. 6 The cyclic voltammetry response of **a** bare SPE and PANINS@rGO/SPCE with presence and absence of glucose. **b** CVs of PANINS@rGO/SPCE at different scan rates (10, 20, 40, 60, 80

and 100 mV s^{-1}) in the presence of 1 mM glucose **c** Square root of different scan rates vs. Current **d** CVs of PANINS/rGO in the presence of 1 to 10 mM glucose concentration

in NMP. The higher the solubility of the materials being dissolved, the higher the conductivity, thereby increases in electrode sensitivity. However, there is no noticeable oxidation peaks of PANINS@rGO/SPCE were observed in absence of glucose in 0.1 M NaOH. This means higher solvency leads to more solubility of the PANI materials and therefore the conductivity, and in turn the electrode sensitivity, increases. The sensitivity of the PANI in NMP is shown and also compared with DMSO and DMF solvents in Supplementary data (S1).

3.2 Effect of scan rate

Figure 6b shows the CVs of PANINS@rGO/SPCE recorded at different scan rates from 5 to 100 mV s^{-1} in a 0.1 M NaOH electrolyte in the presence of 1 mM of glucose. Increase the redox peak current of PANINS@rGO/SPCE with increasing the scan rate. At the scan rate of 60 mV/s redox maximum peak shifts absorbed, oxidation peak showed the positive shift and reduction peak has shown negative shifts with $R^2=0.984$ and $R^2=0.986$, respectively.

3.3 Electrocatalytic characteristics of PANINS@rGO/SPCE

In this present work, as-prepared PANINS/rGO composite has been used for electrocatalytic oxidation of glucose. Electron transfer pathways occurred at PANINS@rGO/SPCE in the following reactions. The basic reaction mechanism between NaOH and PANIN/rGO/SPCE with glucose is as follows and shown in Fig. 7.

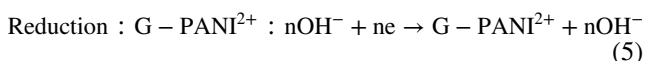
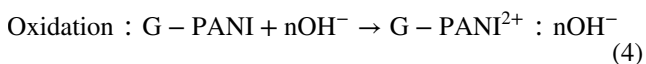
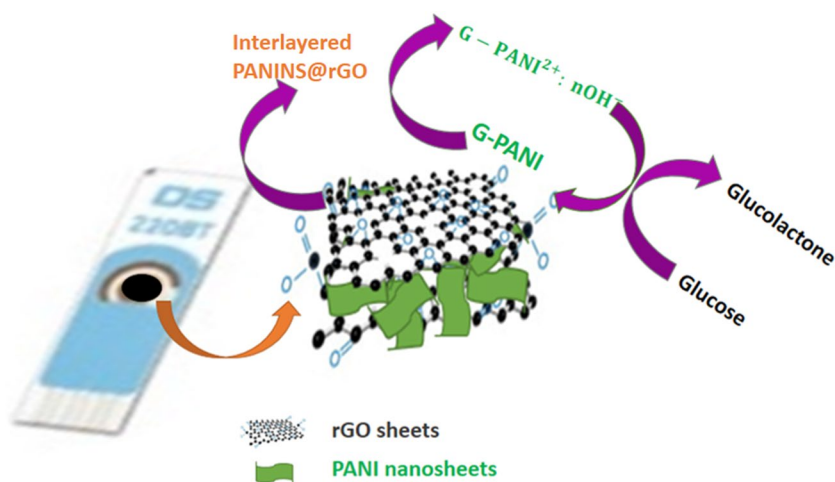
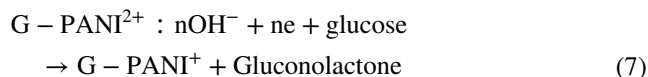


Fig. 7 Non-enzymatic glucose sensing of Interlayered PANINS@rGO



Glucose Mechanism



3.4 Effect of concentration

Furthermore, the electron mobility between 0.1 M NaOH electrolyte and PANINS@rGO/SPCE electrode with various concentrations of glucose ranging from 1 to 10 mM was recorded using CV at a scan rate of 60 mV s^{-1} with a potential range of -0.2 to 0.8 V shown in Fig. 6d. The electrochemical oxidation of anodic peak and the cathodic peak was increased with the increasing glucose concentration. The main factors for catalytic oxidation were mainly due to particle size and specific surface area which give more electrical signal transformation through active sites. For PANINS@rGO, the solubility of PANINS can be affected by interaction among PANI chains and associated counter ions and (Organic) solvents including NMP. Thus, the interactive effect can result in enriched performance for glucose sensing, specifying that the modified electrode can be applied for low-level glucose detection.

3.5 The amperometric response of PANINS@rGO towards glucose

Figure 8a shows the amperometric response of current versus time from 1 to 1000 μM in 0.1 M NaOH solution at the response time within <3 s. After addition of glucose repeatedly, modified PANINS@rGO/SPCE exhibits a step-wise graph with a rise in current. The current-time step graph response mainly depends on the glucose concentration present in the electrolyte solution. Figure 8b shows the

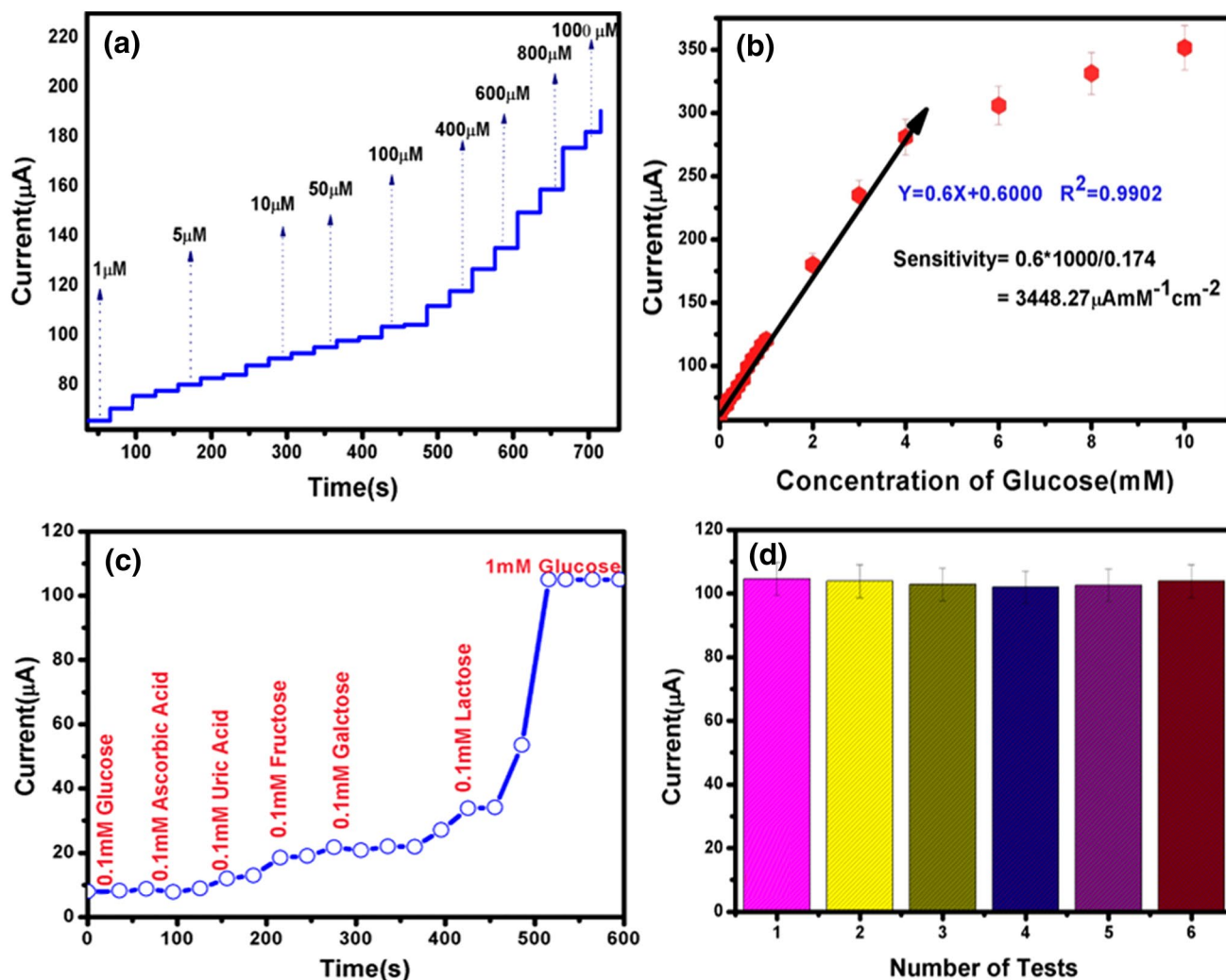


Fig. 8 a Amperometric current vs. time curve of 1–4000 μM of PANINS@rGO/SPE. b Calibration plot of steady-state current vs. concentration of glucose (c). Amperometric response ($i-t$) curve for

PANINS@rGO/SPCE to the glucose and interfering substances. c Repeatability of PANINS@rGO (6 tests)

calibration plots of PANINS@rGO where the concentration of glucose versus current and sensitivity was calculated by the slope of the calibration curve and active surface area of the electrode (the equation is shown below). The graph showed better linearity from 1 to 4 mM with high sensitivity of $3448.27 \mu\text{A mM}^{-1} \text{Cm}^{-2}$ and calculated limited detection (LOD) was $0.03 \mu\text{M}$ where considered ($S/N=3$). The low detection limit of glucose, sensitivity, linear range compared with existing literature as shown in Table 2. The PANINS sheets showed good catalytic activity [29] and interlaying of these sheets at rGO improved the catalytic activity towards the glucose oxidation, LOD, due to the large

surface area of PANINS@rGO rise the more active sites for the electrocatalytic activity. This proves our PANINS@rGO is a sustainable and high-performance non-enzymatic glucose sensor.

$$\text{Active surface area} = \frac{I_p}{2.69 \times 10^5 \times n^{2/3} \times D^{1/2} \times \vartheta^{1/2} \times C} \quad (8)$$

where I_p is the peak current, C is the bulk concentration of glucose solution, n is a number of electron transfer, D is the diffusion coefficient (1.8×10^{-3}) and ϑ is the scan rate.

Table 2 Comparing the performance of non-enzymatic glucose sensing

Working electrode	Linear range (μM)	The detection limit (μM)	Sensitivity ($\mu\text{A m M}^{-1} \text{ cm}^{-2}$)	References
CuO/PANINS-NF/FTO	0.25 μM to 4.6 mM	0.24	1359	[30]
GOx-graphene/PANINS/AuNPs/GCE	4.0–1.12	0.6	–	[31]
PANINS@CuNi	1–5.6 mM	0.2	1030	[32]
NiHCF/PANINS/graphene	0.001–0.765 mM	0.5	487.33	[33]
NiCo ₂ S ₄ /rGO@PANINS	1–7000 μM	0.14	4.924	[34]
NiO/Au/PANINS/rGO/GCE	90–6000	0.23	–	[35]
AuNPs/PANINS/CC	0.0126–10.0	3.08	150	[36]
PANINS	1–4000 μM	0.04	2003.4	[21]
RGO@PANINS	1–4000 μM	0.03	3448.27	Present work

3.6 Interference study

Furthermore, the capacity of anti-interfering of synthesized PANINS@rGO/SPCE was examined in various electroactive interferences such as AA, UA, Galactose, maltose, fructose and lactose. UA and AA did not pose any obvious effect on the glucose assay. Besides, the addition of Galactose, Fructose, Lactose and Maltose, there was a negligible change in the current seen. However, in the addition of 1 mM of glucose, the apparent current responded as shown in Fig. 8c. The stability and repeatability of PANINS@rGO/SPCE with SD, RSD and LOQ was calculated as 0.99, 0.96 and 0.133 of six successive amperometric ($n = 6$) measurements at room temperature which indicating excellent repeatability as shown in Fig. 8d.

4 Conclusion

In conclusion, interlayered PANINS@rGO was prepared successfully through the solution mixing method. It was confirmed from FESEM and TEM the formation of PANINS@rGO. The Amperometric studies of PANINS@rGO were for the detection of non-enzymatic glucose. The obtained results show that high sensitivity was obtained as 3448.27 $\mu\text{A mM}^{-1} \text{ cm}^{-2}$ with detection limit 30 nM ($S/N = 3$). Therefore PANINS@rGO/SPCE showed high sensitivity and also low detection limit (LOD). Also, PANINS show good electrochemical activity which acts as an electron mediator in the electrocatalytic glucose oxidation with high conductivity which leads to high sensitivity and low detection limit. The synergic effect of interlayered PANINS at rGO layers can provide an improved performance which makes it a promising material for enzyme-free glucose sensing.

Acknowledgements This work was supported by Centre for Nano-science and Technology, Institute of Science Technology, JNTU Hyderabad.

Funding The authors did not receive any research fund or grant from any organization.

Compliance with ethical standards

Conflict of interest The authors declared no potential conflicts of interest with respect to the research, authorship and/or publication of this article.

References

1. Y.J. Zhai, J.H. Li, X.Y. Chu, M.Z. Xu, F.J. Jin, X. Li, X. Fang, Z.P. Wei, X.H. Wang, MoS₂ microflowers based electrochemical sensing platform for non-enzymatic glucose detection. *J. Alloys Compd.* (2016). <https://doi.org/10.1016/j.jallcom.2016.02.130>
2. A.D. Association, Diagnosis and classification of diabetes mellitus. *Diabetes Care* **37**, S81–S90 (2014)
3. D.W. Hwang, S. Lee, M. Seo, T.D. Chung, Recent advances in electrochemical non-enzymatic glucose sensors—a review. *Anal. Chim. Acta* **1033**, 1–34 (2018). <https://doi.org/10.1016/j.aca.2018.05.051>
4. S.A. Zaidi, J.H. Shin, Recent developments in nanostructure based electrochemical glucose sensors. *Talanta* **140**, 30–42 (2016). <https://doi.org/10.1016/j.talanta.2015.11.033>
5. L. Liu, W. Qi, X. Gao, C. Wang, G. Wang, Synergistic effect of metal ion additives on graphitic carbon nitride nanosheet-templated electrodeposition of Cu@CuO for enzyme-free glucose detection. *J. Alloys Compd.* (2018). <https://doi.org/10.1016/j.jallcom.2018.02.19>
6. R. Rebelo, A.I. Barbosa, D. Caballero, I.K. Kwon, J.M. Oliveira, S.C. Kundu, R.L. Reis, V.M. Correlo, 3D biosensors in advanced medical diagnostics of high mortality diseases. *Biosens. Bioelectron.* **130**, 20–39 (2019). <https://doi.org/10.1016/j.bios.2018.12.057>
7. M.S. Steiner, A. Duerkop, O.S. Wolfbeis, Optical methods for sensing glucose. *Chem. Soc. Rev.* **40**, 4805–4839 (2011)
8. P.W. Barone, R.S. Parker, M.S. Strano, In Vivo fluorescence detection of glucose using a single-walled carbon nanotube optical sensor: design, fluorophore properties, advantages, and disadvantages. *Anal. Chem.* **77**, 7556–7562 (2005)

9. J. Luo, P. Luo, M. Xie, K. Du, B. Zhao, F. Pan, P. Fan, F. Zeng, D. Zhang, Z. Zheng, G. Liang, A new type of glucose biosensor based on surface acoustic wave resonator using Mn-doped ZnO multilayer structure. *Biosens. Bioelectron.* **49**, 512–518 (2013)
10. J. Tian, S. Liu, Y. Luo, X. Sun, Fe(III)-based coordination polymer nanoparticles: peroxidase-like catalytic activity and their application to hydrogen peroxide and glucose detection. *Catal. Sci. Technol.* **2**, 432–436 (2012)
11. G. Wang, X. He, L. Wang, A. Gu, Y. Huang, B. Fang, B. Geng, X. Zhang, Non-enzymatic electrochemical sensing of glucose. *Microchim. Acta* **180**, 161–186 (2013)
12. D. Zhai, B. Liu, Y. Shi, L. Pan, Y. Wang, W. Li, R. Zhang, G. Yu, Highly sensitive Glucose sensor based on Pt nanoparticle/polyaniline hydrogel heterostructures. *ACS Nano* **7**, 3540–3546 (2013)
13. X. Kang, J. Wang, H. Wu, I.A. Aksay, J. Liu, Y. Lin, Glucose oxidase-graphene Chitosan modified electrode for direct electrochemistry and glucose sensing. *Biosens. Bioelectron.* **25**, 901–905 (2009)
14. S. Liu, J. Tian, L. Wang, Y. Luo, W. Lu, X. Sun, Self-assembled graphene platelet Glucose oxidase nanostructures for glucose biosensing. *Biosens. Bioelectron.* **26**, 4491–4496 (2011). <https://doi.org/10.1007/s00604-012-0923-1>
15. W.-C. Lee, K.-B. Kim, N.G. Gurudatt, K.K. Hussain, C.S. Choi, D.-S. Park, Y.-B. Shim, Comparison of enzymatic and non-enzymatic glucose sensors based on hierarchical Au-Ni alloy with a conductive polymer. *Biosens. Bioelectron.* (2019). <https://doi.org/10.1016/j.bios.2019.01.028>
16. N. Karikalan, M. Velmurugan, S.M. Chen, C. Karuppiyah, Modern approach to the synthesis of Ni (OH) 2 decorated sulfur doped carbon nanoparticles for the nonenzymatic glucose sensor. *ACS Appl. Mater. Interfaces* **8**, 22545–22553 (2016)
17. S. Radhakrishnan, J. Mathiyarasu, Graphene-carbon nanotubes modified electrochemical sensors, in *Graphene-based electrochemical sensors for biomolecules*, ed. by A. Pandikumar, P. Rameshkumar (Elsevier, Amsterdam, 2019), pp. 187–205
18. A. Mahmoud, M. Echabaane, K. Omri, L. El Mir, R.B. Chaabane, Development of an impedimetric non-enzymatic sensor based on ZnO and Cu doped ZnO nanoparticles for the detection of glucose. *J. Alloys Compd.* **786**, 960–968 (2019). <https://doi.org/10.1016/j.jallcom.2019.02.060>
19. L. Sinha, S. Pakhira, P. Bhojane, S. Mali, C.K. Hong, P.M. Shirage, Hybridization of Co₃O₄ and α-MnO₂ nanostructures for high-performance nonenzymatic glucose sensing. *ACS Sustain. Chem. Eng.* **6**(10), 13248–13261 (2018). <https://doi.org/10.1021/acssuschemeng.8b02835>
20. Y. Xie, Y. Song, Y. Zhang, L. Xu, L. Miao, C. Peng, L. Wang, Cu metalorganic framework-derived Cu Nanospheres@Porous carbon/macroporous carbon for electrochemical sensing glucose. *J. Alloys Compd.* **235**, 97–102 (2018). <https://doi.org/10.1016/j.jallcom.2018.05.064>
21. H. Dai, P. Cao, D. Chen, Y. Li, N. Wang, H. Ma, M. Lin, Ni-Co-S/PPy core-shell nanohybrid on nickel foam as a non-enzymatic electrochemical glucose sensor. *Synth. Met.* **235**, 97–102 (2018). <https://doi.org/10.1016/j.synthmet.2017.12.004>
22. S. Komathi, A.I. Gopalan, N. Muthuchamy, K.P. Lee, Polyaniline nanoflowers grafted onto nanodiamonds via a soft template-guided secondary nucleation process for high-performance glucose sensing. *RSC Adv.* **7**(25), 15342–15351 (2017). <https://doi.org/10.1039/c6ra24760a>
23. K. Justice Babu, S. Sheet, Y.S. Lee, G. Gnana Kumar, Three-dimensional dendrite Cu–Co/reduced graphene oxide architectures on a disposable pencil graphite electrode as an electrochemical sensor for nonenzymatic glucose detection. *ACS Sustain. Chem. Eng.* (2018). <https://doi.org/10.1021/acssuschemeng.7b03314>
24. G.G. Wallace, P.R. Teasdale, G.M. Spinks, L.A. Kane-Maguire, *Conductive electroactive polymers: intelligent materials systems* (CRC Press, Boca Raton, 2002)
25. R. Arukula, M. Vinothkannan, A.R. Kim, D.J. Yoo, Cumulative effect of bimetallic alloy, conductive polymer and graphene toward electrooxidation of methanol: an efficient anode catalyst for direct methanol fuel cells. *J. Alloys Compd.* **771**, 477–488 (2019). <https://doi.org/10.1016/j.jallcom.2018.08.303>
26. M. Jaymand, Recent progress in chemical modification of polyaniline. *Progr. Polym. Sci.* **38**(9), 1287–1306 (2013). <https://doi.org/10.1016/j.progpolymsci.2013.05.015>
27. C. Xiong, T. Li, Y. Zhu, T. Zhao, A. Dang, H. Li, X. Ji, Y. Shang, M. Khan, Two-step approach of fabrication of interconnected nanoporous 3D reduced graphene oxide-carbon nanotube-polyaniline hybrid as a binder-free supercapacitor electrode. *J. Alloys Compd.* **695**, 1248–1259 (2017). <https://doi.org/10.1016/j.jallcom.2016.10.253>
28. H. Wang, L. Ma, M. Gan, T. Zhou, "Design and fabrication of macroporous polyaniline nanorods@ graphene-like MoS₂ nanocomposite with the high electrochemical performance for supercapacitors. *J. Alloys Compd.* **699**, 176–182 (2017). <https://doi.org/10.1016/j.jallcom.2016.12.344>
29. J. Wang, Z. Wu, K. Hu, X. Chen, H. Yin, High conductivity graphene-like MoS₂/polyaniline nanocomposites and its application in a supercapacitor. *J. Alloys Compd.* **619**, 38–43 (2015). <https://doi.org/10.1016/j.jallcom.2014.09.008>
30. Z. Zhou, S. Gu, Y. Zhang, F. Wu, N. Zhou, Lithium storage performance improvement of NaTi₂ (PO₄)₃ with nitrogen-doped carbon derived from Polyaniline, ". *J. Alloys Compd.* **767**, 745–752 (2018)
31. N. Chen, Y. Ren, P. Kong, L. Tan, H. Feng, Y. Luo, In situ one-pot preparation of reduced graphene oxide/polyaniline composite for high-performance electrochemical capacitors. *Appl. Surf. Sci.* **392**, 71–79 (2017). <https://doi.org/10.1016/j.apsusc.2016.07.168>
32. M. Mitra, C. Kulsi, K. Chatterjee, K. Kargupta, S. Ganguly, D. Banerjee, S. Goswami, Reduced graphene oxide-polyaniline composites—synthesis, characterization and optimization for thermoelectric applications. *RSC Adv.* **5**(39), 31039–31048 (2015). <https://doi.org/10.1039/c5ra01794g>
33. A. Bhattacharya, A. De, Conducting polymers in solution—progress toward processibility. *J. Macromol. Sci. C* **39**, 17–56 (1999). <https://doi.org/10.1081/MC-100101416>
34. K. Krukiewicz, A. Katunin, The effect of the reaction medium on the conductivity and morphology of polyaniline doped with camphorsulfonic acid. *A Synth. Met.* **214**, 45–49 (2016). <https://doi.org/10.1016/j.synthmet.2016.01.017>
35. K. Tzou, R.V. Gregory, A method to prepare soluble polyaniline salt solutions—in situ doping of PANI base with organic dopants in polar solvents. *Synth. Met.* **53**(3), 365–377 (1993). [https://doi.org/10.1016/0379-6779\(93\)91106-C](https://doi.org/10.1016/0379-6779(93)91106-C)
36. A. Esmaeeli, A. Ghaffarinejad, A. Zahedi, O. Vahidi, Copper oxide-polyaniline nanofiber modified fluorine doped tin oxide (FTO) electrode as a non-enzymatic glucose sensor. *Sens. Actuators B* **266**, 294–301 (2018)
37. Q. Xu, S.-X. Gu, L. Jin, Y.-E. Zhou, Z. Yang, W. Wang, X. Hu, Graphene/polyaniline/gold nanoparticles nanocomposite for the direct electron transfer of glucose oxidase and glucose biosensing. *Sens. Actuators B* **190**, 562–569 (2014). <https://doi.org/10.1016/j.snb.2013.09.049>
38. S. Bilal, W. Ullah, Polyaniline@ CuNi nanocomposite: a highly selective, stable and efficient electrode material for binder free non-enzymatic glucose sensor. *Electrochim. Acta* **284**, 382–391 (2018). <https://doi.org/10.1016/j.electacta.2018.07.165>
39. Y. Kong, Y. Sha, Y. Tao, Y. Qin, H. Xue, M. Lu, Non-enzymatic glucose sensor based on nickel hexacyanoferrate/

- polyaniline hybrids on graphene prepared by a one-step process. *J. Electrochem. Soc.* **161**(12), B269–B274 (2014). <https://doi.org/10.1149/2.0961412jes>
40. Y. Wang, J. Zhong, F. Ding, Q. Zhao, Z. Zhang, X. Liu, Y. Liu, H. Rao, P. Zou, X. Wang, A bifunctional NiCo₂S₄/reduced graphene oxide@ polyaniline nanocomposite as a highly-efficient electrode for glucose and rutin detection. *New J. Chem.* **42**(12), 9398–9409 (2018). <https://doi.org/10.1039/C8NJ00663F>
 41. K. Ghanbari, F. Ahmadi, NiO hedgehog-like nanostructures/Au/polyaniline nanofibers/reduced graphene oxide nanocomposite with electrocatalytic activity for non-enzymatic detection of glucose. *Anal. Biochem.* **518**, 143–153 (2017). <https://doi.org/10.1016/j.ab.2016.11.020>
 42. M. Xu, Y. Song, Y. Ye, C. Gong, Y. Shen, L. Wang, L. Wang, A novel flexible electrochemical glucose sensor based on gold nanoparticles/polyaniline arrays/carbon cloth electrode. *Sens. Actuators B* **252**, 1187–1193 (2017). <https://doi.org/10.1016/j.snb.2017.07.147>
 43. S. Kailasa, B. Geeta, N. Jayrambabu, R. Kiran Kumar Reddy, S. Sharma, K. Venkateswara Rao, Conductive polyaniline nanosheets (CPANINS) for a non-enzymatic glucose sensor. *Mater. Lett.* **245**, 118–121 (2019). <https://doi.org/10.1016/j.matlet.2019.02.103>
 44. H. Wu, J. Fan, E. Liu, X. Hu, Y. Ma, X. Fan, Y. Li, C. Tang, Facile hydrothermal synthesis of TiO₂ nanospindles-reduced graphene oxide composite with enhanced photocatalytic activity. *J. Alloys Compd.* **623**, 298–303 (2015). <https://doi.org/10.1016/j.jallcom.2014.10.153>
 45. M. Ghorbani, H. Abdizadeh, M.R. Golobostanfard, Reduction of graphene oxide via modified hummers method. *Procedia Mater. Sci.* **11**, 326–330 (2015). <https://doi.org/10.1016/j.mspro.2015.11.104>
 46. W. Zheng, L. Hu, L.Y. Lee, K.Y. Wong, Copper nanoparticles/polyaniline/graphene composite as a highly sensitive electrochemical glucose sensor. *J. Electroanal. Chem.* **781**, 155–160 (2016). <https://doi.org/10.1016/j.jelechem.2016.08.004>
 47. A. Viswanathan, A.N. Shetty, Single-step synthesis of rGO, copper oxide and polyaniline nanocomposites for high energy supercapacitors. *Electrochim. Acta* **289**, 204–217 (2018). <https://doi.org/10.1016/j.electacta.2018.09.033>
 48. Y. Wang, Z. Hua, L. Jia, H. Li, T. Li, C. Kai, Y. Gu, Optimizing the polymerization conditions of soluble polyaniline doped with itaconic acid. *J. Macromol. Sci. A* **51**(7), 577–581 (2014). <https://doi.org/10.1080/10601325.2014.916179>
 49. S. Kailasa et al., Twisted polyaniline nanobelts@ rGO for room temperature NO₂ sensing. *Mater. Lett.* **257**, 126687 (2019)
 50. H. Zeghioud, S. Lamouri, Z. Safidine, M. Belbachir, Chemical synthesis and characterization of highly soluble conducting polyaniline in mixtures of common solvents. *J. Serb. Chem. Soc.* **80**(7), 917–931 (2015). <https://doi.org/10.2298/JSC140719003Z>
 51. A. Chiolerio, S. Bocchini, F. Scaravaggi, S. Porro, D. Perrone, D. Beretta, C.F. Pirri, Synthesis of polyaniline-based inks for inkjet printed devices: electrical characterization highlighting the effect of primary and secondary doping. *Semicond. Sci. Technol.* **30**(10), 104001 (2015). <https://doi.org/10.1088/0268-1242/30/10/104001>

Publisher's Note Springer Nature remains neutral with regard to jurisdictional claims in published maps and institutional affiliations.